

Analyst

Accepted Manuscript



This is an *Accepted Manuscript*, which has been through the Royal Society of Chemistry peer review process and has been accepted for publication.

Accepted Manuscripts are published online shortly after acceptance, before technical editing, formatting and proof reading. Using this free service, authors can make their results available to the community, in citable form, before we publish the edited article. We will replace this *Accepted Manuscript* with the edited and formatted *Advance Article* as soon as it is available.

You can find more information about *Accepted Manuscripts* in the [Information for Authors](#).

Please note that technical editing may introduce minor changes to the text and/or graphics, which may alter content. The journal's standard [Terms & Conditions](#) and the [Ethical guidelines](#) still apply. In no event shall the Royal Society of Chemistry be held responsible for any errors or omissions in this *Accepted Manuscript* or any consequences arising from the use of any information it contains.

COMMUNICATION

Mechanical mapping with chemical specificity by confocal Brillouin and Raman microscopy

Cite this: DOI: 10.1039/x0xx00000x

F. Palombo,^{*a} M. Madami,^b N. Stone^{a,c} and D. Fioretto^b

Received 00th January 2012,

Accepted 00th January 2012

DOI: 10.1039/x0xx00000x

www.rsc.org/analyst

We describe the first application of confocal Brillouin and Raman microscopy to *ex vivo* human epithelial tissue - Barrett's oesophagus. This non-invasive label-free approach provides high-resolution mechanical mapping with chemical specificity, opening the route to a new integrated method for multiple biomedical and bioengineering applications, and potentially *in vivo* real-time diagnostics.

Brillouin spectroscopy, based on the inelastic light scattering from thermally activated acoustic phonons,¹ measures elastic properties of a material. Despite an extensive use in material science,²⁻⁴ Brillouin spectroscopy has only sparingly been applied to biomedical studies, essentially confined to proteins,⁵⁻⁹ eye¹⁰ and bone¹¹ partly due to material transparency. Among biomechanical techniques for tissue structure detection, elastography is especially promising,¹² although improvements are expected in sensitivity and image distortion. Nanoindentation by atomic force microscopy (AFM)¹³ offers enhanced resolution, however it requires contact and suitable tips. Coupling Brillouin spectroscopy to confocal microscopy offers a versatile non-contact method for mechanical mapping at a cellular scale. This approach has been applied to bone^{14,15} and, through advanced imaging, to mice eye¹⁶ and *in vivo* human eye.^{17,18} Probing complex heterogeneous materials such as biological tissues is challenging because spatially resolved chemical information is required. For instance, the composition of atherosclerotic lesions is relevant to understanding the pathogenesis of the disease and clinical outcome. This information can be achieved by vibrational spectroscopy such as Raman scattering or IR absorption when coupled to a microscope.^{19,20} Raman microscopy has the advantage of narrow bands, low scattering of water and short excitation wave lengths, thus it is especially suited for biomedical applications.^{21,22} Here, we describe the first application of confocal Brillouin and Raman microscopy to *ex vivo* epithelial tissues. In this example we explore Barrett's oesophagus, which is a change in the lining of the oesophagus which raises the risk of oesophageal adenocarcinoma by around 100 times.²³ Mechanical mapping of tissue at high spatial

resolution and with added chemical specificity is reported, demonstrating the possibility to combine the two techniques for a simultaneous mechanochemical mapping of biomaterials. This should open up new advances for *in vivo* and real-time diagnosis of pathology.

Brillouin scattering is typically measured in the gigahertz range, thus requiring high-contrast spectrometers with highly monochromatic lasers. A tandem multipass Fabry-Perot interferometer has been introduced to circumvent the problems of low sensitivity and overlapping orders of interference.²⁴ The result is a high-contrast spectrometer of the kind used here.^{25,26} A microfocused approach was applied to the experiment, thus enabling an exquisite level of detail to be gained in mechanical mapping. The drawback of slow measurements may be overcome applying fast scanning techniques in combination with multivariate statistical analysis of the hyperspectral datasets.

In this Communication, we present Brillouin and Raman spectra of glandular material and fibrillar regions forming the *lamina propria* mucosa of Barrett's oesophagus. This shows variations in the measured stiffness across the epithelial tissue at a sub-micrometre level, and how these changes correlate with the local chemical composition and structure. We measured Brillouin spectroscopic maps by point-to-point scanning the surface of the specimen (histological cross-section) and obtained images showing the distribution of different parameters within the damped acoustic oscillator model. Finally, we quantified the acoustic wave attenuation and apparent velocity across a fibrillar region, and demonstrated the complementary between attenuation and frequency shift at this location.

Methods

A freshly excised oesophageal biopsy sample was collected during routine endoscopy, mounted on acetate paper and snap frozen in liquid nitrogen. It was then cryosectioned, mounted on a calcium fluoride substrate and stored in a freezer (−80°C) until required for analysis. It was then removed for the

microscopic analysis. The thickness of the air dried section was approximately 5 μm .

Brillouin spectra were collected with a microfocussed setup²⁶ using a tandem 3+3 Fabry-Perot interferometer.²⁴ We used a single-mode Excelsior Diode-Pumped Solid-State (DPSS) laser with 532 nm wavelength and 5 mW output power measured at the sample. A Zeiss dark-field objective (numerical aperture 0.75, working distance 4.7 mm) focuses the incident laser beam perpendicularly on the surface of the sample and collects the backscattered light which is sent to the interferometer for frequency analysis. LED light with 455 nm wavelength in combination with a CCD camera were used to illuminate the sample at grazing incidence, thus exalting the edges of the structures. The lateral resolution of this setup is approximately 250 nm. The spectral resolution is 0.1 GHz. Spectra were acquired in the range -30 to 30 GHz (-23 to -12 GHz for the two-dimensional map) with 1500 scans per spectrum. The measurement of Brillouin maps required the sample position to be stabilized against lateral drifts, which may occur during long time acquisitions. This is realized selecting a reference area within the illuminated region (through the red-yellow boxes in the figures) and using an image recognition software which supplies a feedback signal to the positioning stage. Approximately 10 minutes per spectrum was the time required to achieve a good signal-to-noise ratio. Fit analysis with a damped harmonic oscillator²⁵ was applied to the spectra.

Raman spectra were collected with a Renishaw system 1000 confocal microscope equipped with an 830 nm laser and a Leica 100 \times objective. The spectrometer was used in semi-confocal mode with a 50 μm slit, backscattered light was dispersed through a 300 grooves/mm grating onto a NIR sensitive deep depletion CCD detector. The spectral resolution was 10 cm^{-1} . Spectra were acquired in the range 300 – 2000 cm^{-1} using a 10 s exposure time and ten accumulations to achieve a good signal-to-noise ratio. A fast scanning approach coupled to state-of-the-art hyperspectral data analyses has been shown to be effective at providing signals sufficient to distinguish tissue type and pathology.²⁰ Attention was paid in obtaining site matched data from both Raman and Brillouin experiments, and this was achieved using patterns of tissue edges. Raman spectra were corrected for the energy sensitivity of the spectrometer using a fluorescent green glass standard, the baseline was subtracted with a 3rd order polynomial fit and the resulting profiles were normalised to the total integrated intensity in the range 500 – 1800 cm^{-1} .

Results and Discussion

Fig. 1 shows a typical Brillouin scattering spectrum of glandular material within the *lamina propria* of *ex vivo* Barrett's oesophagus.

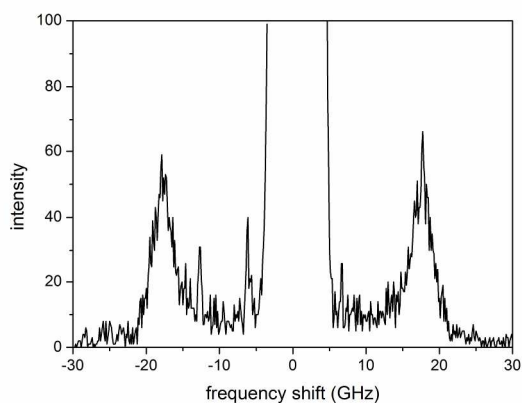


Fig. 1 Brillouin scattering spectrum of glandular material within the *lamina propria* of an *ex vivo* section of Barrett's oesophagus. Brillouin peak maxima are at ± 19 GHz. The narrow peaks at about 6.5 GHz and 13.0 GHz are due to weak extra-modes of the laser.

The spectrum presents an intense central peak due to the elastic scattering and a set of equally shifted peaks, which are the Stokes and anti-Stokes parts of a Brillouin doublet. In an elastic medium, the Brillouin doublet is predicted at frequency shift $\omega = \pm cq$ with respect to the elastic peak, where c is the acoustic wave velocity and $q = 2nk_i$ the momentum exchanged in the backscattering process, with n the refractive index of the material and k_i the wave vector of

the incident light.²⁵ The line broadening observed in Fig. 1, originating from damped acoustic modes, indicates the viscoelastic nature of the material which is related to the presence of hydration water. Bound water is known to be a key constituent of tissues and is especially relevant to protein structure and aggregates. In this condition, the apparent sound velocity is obtained by the characteristic frequency ω_b of a damped harmonic oscillator²⁵ as $c = \omega_b/q$.

To define the chemical composition, micro-Raman spectra of the epithelial tissue were also measured (Fig. 2).

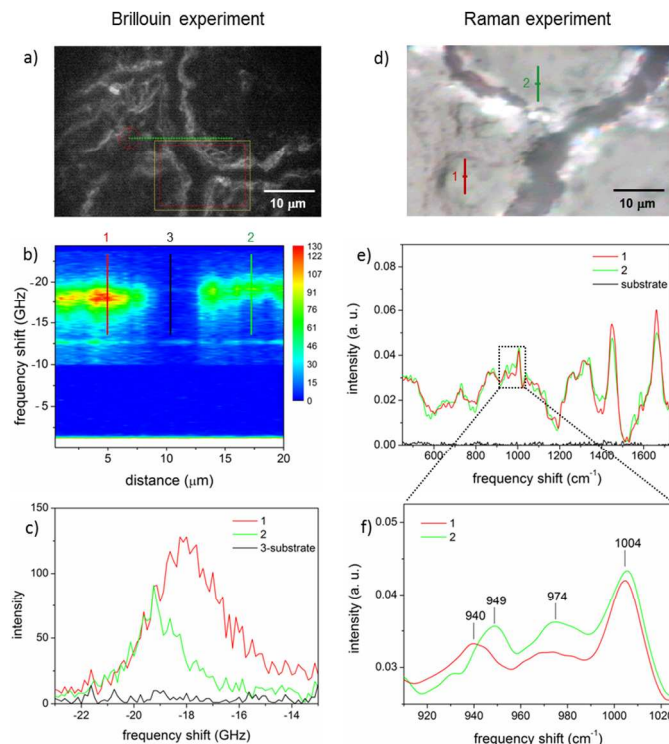


Fig. 2 (a) Optical image of a gland/connective tissue interface of Barrett's oesophagus acquired with dark-field illumination. Parallel fibrils are visible on the left hand side. The dotted green line indicates a 20 μm segment along which Brillouin spectra were measured every 0.5 μm . The red-yellow boxes define a reference area for sample stabilization. (b) Intensity distribution of stacked Brillouin spectra across the scanned segment. Lines identify selected spectra (c). (d) Optical image acquired with white light illumination. Numbers indicate the regions from which a Raman spectrum was extracted (e). (f) Expanded view of the C–C stretching region. Numbers indicate the wavenumber in the observed resonances (see text).

Figs. 2(a,d) show optical images of the regions analysed by confocal Brillouin and Raman microscopy. The morphology of the specimen is clearly visualised in dark-field illumination (Fig. 2a), which exalts the edges of tissue structures. A fibrous/non-fibrous interface was the region selected for characterization. The dark branched pattern across both images was identified as the calcium fluoride substrate, having no signal in these spectral regions (black spectrum in Figs. 2c,e). An intensity map of Brillouin spectra collected through a linear scan across the interface is displayed in Fig. 2(b). Selected spectra from distinct parts of the interface show differences in the Brillouin peak (Fig. 2c), with the fibrous region (red spectrum) having a higher intensity and lower frequency peak than the non-fibrous one (green spectrum). Raman spectra from regions either side of the interface in Fig. 2(d) are complex and denote a combination of biochemical constituents (Fig. 2e). Spectral assignment based on previous studies^{19-23, 27, 28} revealed a proline-rich composition (peaks at 727 , 860 and 972 cm^{-1} , due to coupled =C–H bending and C–C stretching modes) which plausibly corresponds to type I collagen forming fibrils (Fig. 2a) within the extracellular matrix. On the other hand, spectrum 2 shows

characteristic peaks of nucleic acids (DNA backbone at 1058 and purine bases at 1587 cm^{-1}) and therefore it can be assigned to epithelial cells. A more accurate analysis of tissue constituents will be the focus of a further work aimed at extending the results of the present feasibility study. Fig. 2(f) shows a zoom of the spectra in the C–C stretching region. Here, a peak at 940 cm^{-1} in spectrum 1 identifies hydrated type I collagen.²⁹ The presence of hydration water in the fibrils is discussed below. By analogy, the peak at 949 cm^{-1} in spectrum 2 may be assigned to free (non-water bound) carbon backbones.

Micro-Brillouin two-dimensional mapping of a structured glandular region was also performed (Fig. 3).

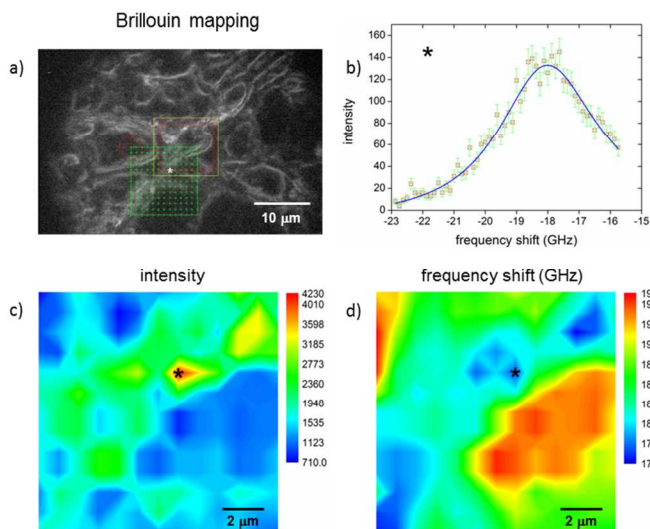


Fig. 3 (a) Optical image of a glandular region of Barrett's oesophagus acquired with dark-field illumination. A fibrous matrix embedding oval-shaped structures (cells) is visible therein. The dotted green box indicates an area of $12 \times 12\ \mu\text{m}^2$ where Brillouin spectra were acquired using a $1\ \mu\text{m}$ step-size. The red-yellow boxes define a reference area for sample stabilization. The asterisk is the location from which a Brillouin spectrum was extracted (b): symbols indicate the measured spectrum whilst the blue line is the result of a least-square fit with a damped harmonic oscillator function. (c,d) Images showing the distribution of fitted intensity and frequency shift of the Brillouin peak across the scanned area.

Fig. 3(a) is an optical image of the tissue at this location, showing oval-shaped cells, embedded in a fibrous matrix. A Brillouin map was acquired from an area of the specimen including both constituents. Fig. 3(b) shows a selected spectrum extracted from a fibrillar region and related fit analysis using a damped harmonic oscillator model (see Methods). Fit results were plotted across the scanned area and Figs. 3(c,d) were obtained. They show the heterogeneous tissue structure through complementary images of the Brillouin peak integrated intensity (Fig. 3c) and frequency shift (Fig. 3d). It can be seen that higher scattering regions correspond to lower frequency ones and *vice versa* (see also Fig. 2c). We can assign the red-to-green regions in Fig. 3(c) to the fibrous matrix of the connective tissue, whilst red-to-green regions in Fig. 3(d) correspond to epithelial cells. This assignment is in line with previous results of histological imaging of epithelial tissue.²⁰ To quantify the attenuation and apparent velocity of the acoustic waves across the same area, we derived the images in Fig. 4.

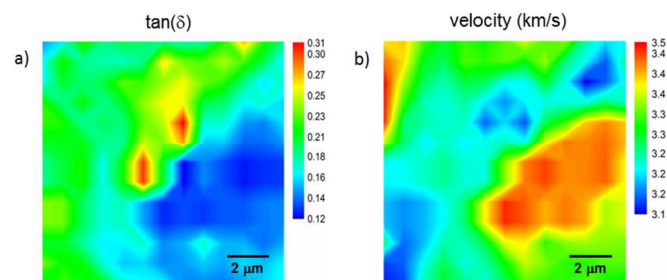


Fig. 4 Images showing the distribution of (a) $\tan(\delta)$ and (b) acoustic wave apparent velocity across the scanned area shown in Fig. 3a. $\tan(\delta)$, the ratio of imaginary-to-real part of the elastic modulus, was obtained as the ratio of fitted width-to-frequency of the Brillouin peak and shows relatively high values in correspondence of broader Brillouin peak, meaning stronger acoustic wave attenuation. The apparent velocity was derived from the fitted Brillouin peak frequency and shows a complementary distribution to that of $\tan(\delta)$, indicating higher velocity in correspondence of lower attenuation of the acoustic waves and *vice versa*.

We obtained $\tan(\delta)$, the ratio of imaginary-to-real part of the elastic modulus, as a ratio of width-to-frequency of the Brillouin peak.³⁰ This quantifies the acoustic wave attenuation across the measured region of the sample. The image in Fig. 4(a) corresponds to that of the peak width distribution (the stronger the attenuation the broader the peak; data not shown). Taking $n = 1.5$ as the refractive index of the tissue,³¹ we also computed the apparent velocity of the acoustic wave ($c = \omega_p/q$) across this region (Fig. 4b) and found a complementarity with the attenuation image (Fig. 4a). A lower velocity is correlated to a stronger attenuation (broader peak), hence suggesting a plasticizing effect of hydration water within the fibrous collagen-rich matrix of the epithelial tissue, i.e. a shift of the structural relaxation to higher frequencies with increasing water content. The structural relaxation is ubiquitous in glass-forming materials²⁵ and, in our sample, is expected to give the maximum of attenuation and velocity dispersion in the MHz frequency region. An increase of concentration of water can move the dispersion region toward the GHz range here explored by Brillouin light scattering, thus decreasing sound velocity and increasing attenuation. Water is key to the conformation and structure of collagen in tissues. Upon cryosectioning, the water content of a tissue drastically changes. There is essentially no bulk water left in air dried tissue sections. However, collagen-bound water may still be present (as well as some rehydration water depending on humidity conditions). Here, higher Brillouin scattering intensity (Fig. 3c) associated with lower acoustic velocity (Fig. 4b) suggests a swelling of the tissue due to collagen-bound water within fibrillar regions. The opposite - lower scattering intensity with higher velocity - is observed for epithelial cells in this cross-section.

Conclusions

We described the first application of confocal Brillouin and Raman microscopy to *ex vivo* epithelial tissues, in this case Barrett's oesophagus. A characterization of the tissue stiffness, composition and their variations across the *lamina propria* mucosa was obtained. Brillouin scattering spectra, originating from damped acoustic phonons, revealed the viscoelastic nature of the material putatively due to water hydration. The evidence of hydrated (type I) collagen fibrils forming the extracellular matrix and of embedded epithelial cells was provided by Raman scattering spectra at a gland/connective tissue interface. The heterogeneity in tissue structure, stiffness and composition

was then identified through this high resolution approach. While the elasticity is expected to change following excision from the living organ (then cryosectioning and air drying), the method revealed changes in the tissue at a cellular level and is therefore a valuable tool for histological analysis. Micro-Brillouin mapping of a glandular region of Barrett's oesophagus showed signatures of high scattering intensity in correspondence of low frequency shift, and this was attributed to the specificity in water hydration. Quantitative results in terms of acoustic wave attenuation and apparent velocity were obtained, thus highlighting the role of bound water within collagen fibrils. The observed anti-correlation between velocity and attenuation suggests that hydration water has a plasticizing effect on the collagen-rich connective tissue which is revealed through a blue-shift of structural relaxation frequencies with increasing the water content.

These results demonstrate the feasibility of applying a combined micro-Brillouin/Raman methodology to simultaneously map the mechanical, structural and chemical properties of biomedical tissues. No fixative or cryopreservative was used in sample preparation, however the effect of different procedures will be investigated in a further study. The method has potential for *in vivo* diagnosis³²⁻³⁴ of pathology, for example atherosclerosis which involves elasticity changes as well as altered structure and composition of the arterial wall.³⁵⁻³⁷ However, this is likely to be implemented using bimodal point measurements initially, with further technological advances required to enable *in vivo* imaging.

Acknowledgements

The authors would like to thank Prof Hugh Barr, Prof Neil Shepherd and Dr Catherine Kendall in the Biophotonics Research Group at Gloucestershire Hospital NHS Foundation Trust for help with the sample collection and preparation.

Notes and references

^a University of Exeter, School of Physics, Exeter EX4 4QJ, UK.

^b University of Perugia, Department of Physics, Perugia I-06100, Italy.

^c Gloucestershire Hospital NHS Foundation Trust, Gloucester GL1 3NN, UK.

- 1 L. Brillouin, *Ann. Phys.*, 1922, **17**, 88-122.
- 2 J. R. Sandercock, in *Light Scattering in Solids III*, eds. M. Cardona and G. Güntherodt, Springer Berlin Heidelberg, 1982, **51**, 173-206.
- 3 M. Madami, S. Bonetti, G. Consolo, S. Tacchi, G. Carlotti, G. Gubbiotti, F. B. Mancoff, M. A. Yar and J. Akerman, *Nature nanotech.*, 2011, **6**, 635-638.
- 4 S. Tacchi, G. Duerr, J. W. Klos, M. Madami, S. Neusser, G. Gubbiotti, G. Carlotti, M. Krawczyk and D. Grundler, *Phys. Rev. Lett.*, 2012, **109**, 137202.
- 5 R. Harley, D. James, A. Miller and J. W. White, *Nature*, 1977, **267**, 285-287.
- 6 J. Randall, J. M. Vaughan and S. Cusack, *Philos. T. Roy. Soc. A*, 1979, **293**, 341-348.
- 7 S. Cusack and A. Miller, *J. Mol. Biol.*, 1979, **135**, 39-51.
- 8 S. Speziale, F. Jiang, C. L. Caylor, S. Kriminski, C. S. Zha, R. E. Thorne and T. S. Duffy, *Biophys. J.*, 2003, **85**, 3202-3213.
- 9 C. Morin, C. Hellmich and P. Henits, *J. Theor. Biol.*, 2013, **317**, 384-393.
- 10 J. M. Vaughan and J. T. Randall, *Nature*, 1980, **284**, 489-491.
- 11 S. Lees, N. J. Tao and S. M. Lindsay, *Connect. Tissue Res.*, 1990, **24**, 187-205.
- 12 J. Ophir, S. K. Alam, B. Garra, F. Kallel, E. Konofagou, T. Krouskop, C. B. Merritt, R. Righetti, R. Souchon, S. Srinivasan and T. Varghese, *J. Med. Ultrasonics*, 2002, **29**, 155-171.
- 13 M. P. E. Wenger, L. Bozec, M. A. Horton and P. Mesquida, *Biophys. J.*, 2007, **93**, 1255-1263.
- 14 M. Kawabe, K. Fukui, M. Matsukawa, M. Granke, A. Saïed, Q. Grimal and P. Laugier, *J. Acoust. Soc. Am.*, 2012, **132**, EL54-EL60.
- 15 M. Matsukawa, R. Tsubota, M. Kawabe and K. Fukui, *Ultrasonics*, 2013.
- 16 G. Scarcelli and S. H. Yun, *Nature Photon.*, 2007, **2**, 39-43.
- 17 S. Reiß, G. Burau, O. Stachs, R. Guthoff and H. Stolz, *Biomed. Opt. Express*, 2011, **2**, 2144-2159.
- 18 G. Scarcelli and S. H. Yun, *Opt. Express*, 2012, **20**, 9197-9202.
- 19 C. Kendall, M. Isabelle, F. Bazant-Hegemark, J. Hutchings, L. Orr, J. Babrah, R. Baker and N. Stone, *Analyst*, 2009, **134**, 1029-1045.
- 20 G. R. Lloyd, J. Wood, C. Kendall, T. Cook, N. Shepherd and N. Stone, *Vib. Spectrosc.*, 2012, **60**, 43-49.
- 21 N. Stone, C. Kendall, N. Shepherd, P. Crow and H. Barr, *J. Raman Spectrosc.*, 2002, **33**, 564-573.
- 22 N. Stone, C. Kendall, J. Smith, P. Crow and H. Barr, *Faraday Discuss.*, 2004, **126**, 141-157; discussion 169-183.
- 23 C. Kendall, N. Stone, N. Shepherd, K. Geboes, B. Warren, R. Bennett and H. Barr, *J. Pathol.*, 2003, **200**, 602-609.
- 24 S. M. Lindsay, M. W. Anderson and J. R. Sandercock, *Rev. Sci. Instrum.*, 1981, **52**, 1478-1486.
- 25 L. Comez, C. Masciovecchio, G. Monaco and D. Fioretto, in *Solid State Physics*, eds. E. C. Robert and L. S. Robert, Academic Press, 2012, **63**, 1-77.
- 26 M. Madami, G. Gubbiotti, S. Tacchi and G. Carlotti, in *Solid State Physics*, eds. E. C. Robert and L. S. Robert, Academic Press, 2012, **63**, 79-150.
- 27 G. Shetty, C. Kendall, N. Shepherd, N. Stone and H. Barr, *Brit. J. Cancer*, 2006, **94**, 1460-1464.
- 28 C. Bielecki, T. W. Bocklitz, M. Schmitt, C. Krafft, C. Marquardt, A. Gharbi, T. Knosel, A. Stallmach and J. Popp, *J. Biomed. Opt.*, 2012, **17**.
- 29 Q. Zhang, K. L. Andrew Chan, G. Zhang, T. Gillece, L. Senak, D. J. Moore, R. Mendelsohn and C. R. Flach, *Biopolymers*, 2011, **95**, 607-615.
- 30 D. Fioretto, L. Comez, G. Socino, L. Verdini, S. Corezzi and P. A. Rolla, *Phys. Rev. E*, 1999, **59**, 1899-1907.
- 31 V. Tsenova and E. V. Stoykova, *Proc. SPIE 5226*, 12th International School on Quantum Electronics: Laser Physics and Applications, 413, 2003.
- 32 J. C. Day, R. Bennett, B. Smith, C. Kendall, J. Hutchings, G. M. Meaden, C. Born, S. Yu and N. Stone, *Phys. Med. Biol.*, 2009, **54**, 7077-7087.
- 33 J. C. Day and N. Stone, *Appl. Spectrosc.*, 2013, **67**, 349-354.

Journal Name

- 34 L. M. Almond, J. Hutchings, C. Kendall, J. C. Day, O. A. Stevens, G. R. Lloyd, N. A. Shepherd, H. Barr and N. Stone, *J. Biomed. Opt.*, 2012, **17**, 081421-081421.
- 35 F. Palombo, S. G. Cremers, P. D. Weinberg and S. G. Kazarian, *J. R. Soc. Interface*, 2009, **6**, 669-680.
- 36 F. Palombo, C. B. Danoux, P. D. Weinberg and S. G. Kazarian, *J. Biomed. Opt.*, 2009, **14**, 044008.
- 37 F. Palombo, H. Shen, L. E. S. Benguigui, S. G. Kazarian and R. K. Upmacis, *Analyst*, 2009, **134**, 1107-1118.